University of Pennsylvania
ScholarlyCommons

Departmental Papers (MEAM)

Department of Mechanical Engineering & Applied Mechanics

3-15-2004

The dielectrophoresis of cylindrical and spherical particles submerged in shells and in semi-infinite media

Hui Liu
University of Pennsylvania

Haim H. Bau
University of Pennsylvania, bau@seas.upenn.edu

Copyright (2004) American Institute of Physics. This article may be downloaded for personal use only. Any other use requires prior permission of the author and the American Institute of Physics.
Reprinted from *Physics of Fluids*, Volume 16, Issue 5, pages 1217-1228.
Publisher URL: http://dx.doi.org/10.1063/1.1649237

This paper is posted at ScholarlyCommons. http://repository.upenn.edu/meam_papers/109
For more information, please contact repository@pobox.upenn.edu.

The dielectrophoresis of cylindrical and spherical particles submerged in shells and in semi-infinite media

Abstract
The dielectrophoretic forces acting on and the resulting velocities of cylindrical and spherical particles embedded in perfectly dielectric viscous fluids are calculated analytically. The fluids are confined in cylindrical/spherical shells and in semi-infinite media with prescribed potential distributions along the surfaces of the media. The forces are calculated by evaluating the Maxwell stress tensor. The velocities of the particles are obtained by solving the Stokes equation for creeping flow. The range of validity of force calculations based on the dipole-moment approximation is estimated.

Keywords
creeping flow, Navier-Stokes equations, electrophoresis

Comments
Copyright (2004) American Institute of Physics. This article may be downloaded for personal use only. Any other use requires prior permission of the author and the American Institute of Physics.
Reprinted from *Physics of Fluids*, Volume 16, Issue 5, pages 1217-1228.
Publisher URL: http://dx.doi.org/10.1063/1.1649237

This journal article is available at ScholarlyCommons: http://repository.upenn.edu/meam_papers/109

HTML ABSTRACT + LINKS

The dielectrophoresis of cylindrical and spherical particles submerged in shells and in semi-infinite media

Hui Liu and Haim H. Bau[a)]
Department of Mechanical Engineering and Applied Mechanics, University of Pennsylvania, Philadelphia, Pennsylvania 19104-6315

(Received 13 August 2003; accepted 29 December 2003; published online 15 March 2004)

The dielectrophoretic forces acting on and the resulting velocities of cylindrical and spherical particles embedded in perfectly dielectric viscous fluids are calculated analytically. The fluids are confined in cylindrical/spherical shells and in semi-infinite media with prescribed potential distributions along the surfaces of the media. The forces are calculated by evaluating the Maxwell stress tensor. The velocities of the particles are obtained by solving the Stokes equation for creeping flow. The range of validity of force calculations based on the dipole-moment approximation is estimated. © *2004 American Institute of Physics.* [DOI: 10.1063/1.1649237]

I. INTRODUCTION

Dielectrophoresis (DEP) is the motion of uncharged polarizable particles in a nonuniform electric field.[1,2] The dielectrophoretic forces result from the interaction of the electric field with the induced dipole moment. Depending on the dielectric properties of the particle and the medium, the motion is directed either toward (positive DEP) or away from (negative DEP) regions of high electric-field intensity. While DEP occurs in both DC and AC electric fields, AC fields are often preferred in order to suppress undesired electrochemical interactions at the surfaces of the electrodes, suppress electrophoresis, and eliminate motion due to the electric charge of the particles. In addition, the use of AC potential allows for capacitive actuation of the electrodes, which prevents the electrodes and particles from burning out when the gap between two electrodes is bridged by conducting particles.[3] DEP is particularly well suited for microfluidic applications and nanoassembly. One can readily control the direction of the electric field by the judicious patterning of the electrodes on the substrate, and high intensity electric fields can be obtained with relatively low potential differences given the small gaps among the actuating electrodes.

DEP has been used for the separation of heterogeneous populations of biological cells and particles into homogeneous subgroups and for the trapping of nanoparticles,[4,5] nanorods, nanofibers,[6] deoxyribonucleic acid,[7] and macromolecules. More recently, DEP was used to separate metallic and semiconducting single-walled nanotubes.[8]

Our interest in DEP is motivated by our work on the transport of liquids through nanotubes. In this work, we trap nanotubes and nanofibers in the gaps between pairs of electrodes patterned on the surfaces of glass and silicon wafers. In order to better design the layout and process conditions of the electrodes, we attempt to simulate the trapping process. We felt that it would be desirable to have a few canonical solutions that can be used to verify the numerical codes—hence this paper.

The dielectrophoretic force is usually approximated through its first dipole moment contribution:[2,9–11]

$$\mathbf{F} \sim \lambda \varepsilon_0 \varepsilon_m V_p \,\mathrm{Re}(f_{\mathrm{CM}}) \nabla |\mathbf{E}_{\mathrm{rms}}^2|, \tag{1}$$

where $\mathbf{E}$ is the electric field; ε_0 and ε_m are, respectively, the dielectric constant of free space and the relative dielectric constant of the suspending liquid, V_p is the volume of the particle, λ is a numerical coefficient on the order of unity, and $\mathrm{Re}(f_{\mathrm{CM}})$ is the real part of the relative particle polarization (i.e., the Clausius–Mossotti factor). Both λ and f_{CM} depend on the geometry of the particle. For example, in the case of a spherical particle, $f_{\mathrm{CM}} = (\varepsilon_p^* - \varepsilon_m^*)/(\varepsilon_p^* + 2\varepsilon_m^*)$ and $\lambda = 3/2$, where ε_p^* and ε_m^* are the complex permittivities of the particle and of the medium, respectively; $\varepsilon^* = \varepsilon - j\sigma/\omega$; and σ is the electric conductivity. The dipole moment approximation is valid only when the dimensions of the particle are much smaller than the characteristic length scale of the electric field. Unfortunately, this is not the case in our application where the size of the tube is comparable to the gap size between the electrodes. Instead, we must calculate the DEP forces by evaluating the Maxwell stress tensor.[12]

There are just a few exact solutions available for the dielectrophoretic motion of particles. In this paper, we analytically solve a few canonical problems. Our objectives are to gain insights to the dielectrophoretic migration, develop a set of benchmark problems that can be used to verify numerical codes, and delineate the range of validity of the dipole moment approximation.

In the first part of this paper, we study the dielectrophoresis of two-dimensional cylindrical particles submerged in cylindrical shells filled with viscous liquid. Since we employ bicylindrical coordinates, we obtain the case of a cylindrical particle submerged in a semi-infinite liquid medium as a special case. In the second part of the paper, we focus on spherical particles embedded in semi-infinite liquid media. In all of these cases, we specify nonuniform potential distributions along the surfaces of the media, compute the polariza-

[a)]Author to whom correspondence should be addressed; electronic mail: bau@seas.upenn.edu

 © 2004 American Institute of Physics

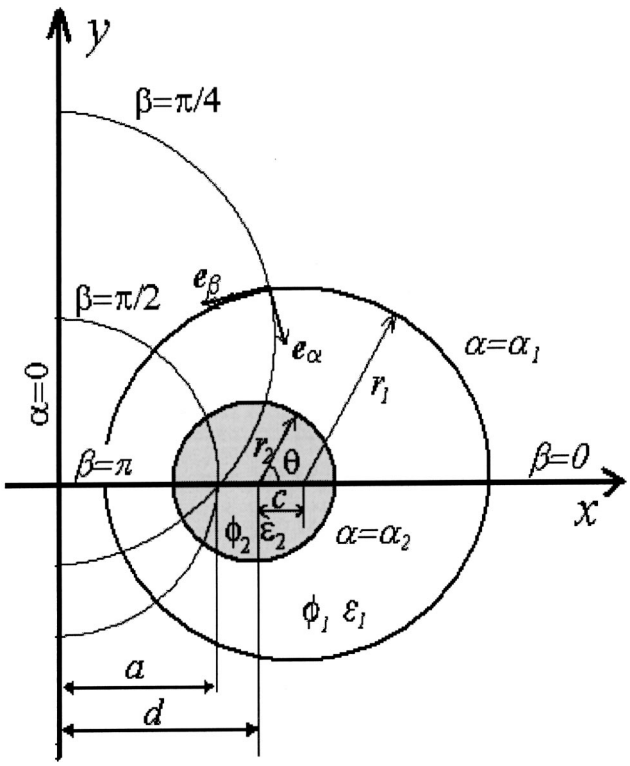

FIG. 1. A schematic depiction of the mathematical model.

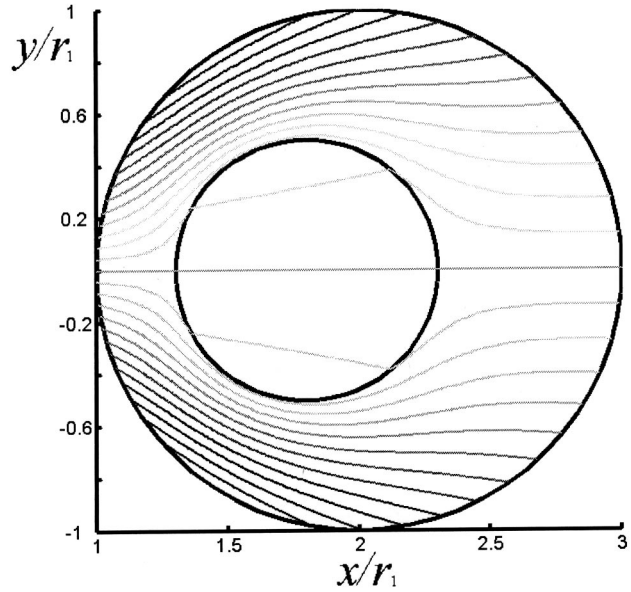

FIG. 2. The potential field (contour lines) when $r_2/r_1=0.5$, $c/r_1=0.2$, and $\varepsilon_2/\varepsilon_1=10$.

tion forces, and compare the exact force values to the values obtained with the dipole moment approximation. Additionally, by equating the DEP forces with the viscous drag acting on the particles, we obtain expressions for the instantaneous velocities of the particles. These motion equations are subsequently integrated to obtain the trajectories of the particles.

II. MATHEMATICAL MODEL

Consider cylindrical and spherical particles located, respectively, inside cylindrical and spherical shells. The radius of the particle is r_2 and the radius of the shell is r_1. The center of the particle is displaced distance c from the center of the shell. See Fig. 1 for a schematic description of the mathematical model. In the limit of r_1 and c approaching infinity, we obtain the case of a particle embedded in a semi-infinite medium. We denote the region between the shell and the particle as domain 1, and the region inside the particle as domain 2. The properties of regions 1 and 2 are denoted, respectively, with subscripts 1 and 2. The electric potential on the surface of the shell is specified, and it is assumed to be piecewise continuous and expandable into a Fourier series. The resulting potential fields in domains 1 and 2 are denoted, respectively, ϕ_1 and ϕ_2. To obtain the potential field in each domain, we solve the Laplace equations:

$$\nabla^2\phi_i=0 \quad (i=1,2). \tag{2}$$

The interfacial boundary conditions on the surface of the particle are

$$\phi_1=\phi_2 \tag{3}$$

and

$$\varepsilon_1\nabla\phi_1\cdot\mathbf{n}=\varepsilon_2\nabla\phi_2\cdot\mathbf{n}, \tag{4}$$

where $\mathbf{n}$ is an outer unit vector normal to the surface of the particle and ε_i is the relative permittivity of domain i. $\varepsilon_0=8.8542\times10^{-12}$ F/m is the permittivity of free space.

We define the length scale of the electric field $L_E=|\mathbf{E}_{0,c}/\nabla\mathbf{E}_{0,c}|$. $\mathbf{E}_0=-\nabla\phi_0$ is the electric field in the absence of a particle, and subscript c indicates that the various quantities are evaluated at the location of the center of the particle. In order to compare the characteristic length of the electric field with the diameter of the particle, we define the dimensionless parameter $H=L_E/2r_2$.

The geometry suggests the use of bicylindrical and bispherical coordinates.[13] These coordinates allow one to specify the boundary conditions at fixed coordinate values. Below, we separately consider the planar and three-dimensional cases.

III. CYLINDRICAL PARTICLE EMBEDDED IN A CYLINDRICAL SHELL

We first consider the planar case. The bicylindrical coordinate system consists of two orthogonal families of circles (Fig. 1). One family of circles corresponds to constant value α coordinates $(0\leqslant\alpha_1\leqslant\alpha\leqslant\alpha_2<\infty)$. The surfaces of the shell and particle are, respectively, at $\alpha=\alpha_1$ and $\alpha=\alpha_2$. The second family of circles corresponds to constant β $(-\pi\leqslant\beta\leqslant\pi)$ coordinates. The case of the semi-infinite medium is obtained by setting $\alpha_1=0$.

The relationship between the Cartesian coordinates (x, y) transverse to the axis and the bicylindrical coordinates (α,β) is given by

$$x+iy=a\coth\left(\frac{1}{2}(\alpha-i\beta)\right), \tag{5}$$

where $a=(M^2-r_1^2)^{1/2}$, $M=(r_1^2-r_2^2+c^2)/2c$, $\alpha_1=1/2\ln[(M+a)/(M-a)]$, and $\alpha_2=1/2\ln[(M-c+a)/(M-c-a)]$. The Laplace equation in bicylindrical coordinates is

$$\frac{\partial^2\phi_i}{\partial\alpha^2}+\frac{\partial^2\phi_i}{\partial\beta^2}=0,\quad i=1,2. \tag{6}$$

The given potential distribution $f(\beta)$ on the wall of the tube is expanded into the Fourier series,

$$f(\beta)=\sum_{n=1}^{\infty}[a_n\sin n\beta+b_n\cos n\beta], \tag{7}$$

where $a_n=1/\pi\int_{-\pi}^{\pi}f(t)\sin(nt)dt$ and $b_n=1/\pi\int_{-\pi}^{\pi}f(t)\cos(nt)dt$ $(n=1,2,....)$. Without loss of generality, we scale the average surface potential to zero. In practice, one could approximate the surface potential distribution by patterning individually controlled electrodes on the surface.

The electric potentials are

$$\phi_1=\sum_{n=1}^{\infty}[(A_ne^{n\alpha}+B_ne^{-n\alpha})\sin n\beta+(C_ne^{n\alpha}+D_ne^{-n\alpha})\cos n\beta] \tag{8}$$

and

$$\phi_2=\sum_{n=1}^{\infty}[X_ne^{-n\alpha}\sin n\beta+Y_ne^{-n\alpha}\cos n\beta]. \tag{9}$$

In the above, $A_n=\chi a_ne^{n\alpha_1}/(\chi e^{2n\alpha_1}+e^{2n\alpha_2})$, $B_n=a_ne^{n(\alpha_1+2\alpha_2)}/(\chi e^{2n\alpha_1}+e^{2n\alpha_2})$, $C_n=\chi b_ne^{n\alpha_1}/(\chi e^{2n\alpha_1}+e^{2n\alpha_2})$, $D_n=b_ne^{n(\alpha_1+2\alpha_2)}/(\chi e^{2n\alpha_1}+e^{2n\alpha_2})$, $X_n=(1+\chi)a_ne^{n(\alpha_1+2\alpha_2)}/(\chi e^{2n\alpha_1}+e^{2n\alpha_2})$, $Y_n=(1+\chi)b_ne^{n(\alpha_1+2\alpha_2)}/(\chi e^{2n\alpha_1}+e^{2n\alpha_2})$, and $\chi=(\varepsilon_1-\varepsilon_2)/(\varepsilon_1+\varepsilon_2)$.

As an example of the potential field, Fig. 2 depicts constant potential lines (contours) when $r_2/r_1=0.5$, $c/r_1=0.2$, $\varepsilon_2/\varepsilon_1=10$, and $f(\beta)=\cos(\beta)$.

A. Force calculation based on virtual work

We will use various methods to calculate the dielectrophoretic forces. Since the medium is a perfect dielectric, we can use the method of virtual work. The total electric energy per unit length of the system is[14]

$$U=\frac{\varepsilon_0}{2}\left(\int\int_{R_1}\varepsilon_1\mathbf{E}_1\cdot\mathbf{E}_1dR_1+\int\int_{R_2}\varepsilon_2\mathbf{E}_2\cdot\mathbf{E}_2dR_2\right), \tag{10}$$

where $\mathbf{E}_1$ and $\mathbf{E}_2$ are, respectively, the electric fields in domains 1 and 2. R_1 and R_2 are, respectively, domains 1 and 2. Upon substituting the electric potentials in (10), we obtain

$$U=\frac{1}{2}\sum_{n=1}^{\infty}\frac{\pi\varepsilon_0\varepsilon_1n(e^{2n\alpha_2}(\varepsilon_1+\varepsilon_2)+e^{2n\alpha_1}(\varepsilon_2-\varepsilon_1))(a_n^2+b_n^2)}{e^{2n\alpha_1}(\varepsilon_1-\varepsilon_2)+e^{2n\alpha_2}(\varepsilon_1+\varepsilon_2)}. \tag{11}$$

Since $\alpha_2>\alpha_1$, as expected, we have $U>0$. The x-direction dielectrophoretic (DEP) force per unit length of the particle is[14]

$$F_x=-\frac{\partial U}{\partial c}=\frac{2\pi\varepsilon_0\varepsilon_1(\varepsilon_1^2-\varepsilon_2^2)}{a}\times\sum_{n=1}^{\infty}\frac{n^2e^{2n(\alpha_1+\alpha_2)}(a_n^2+b_n^2)}{[(\varepsilon_1-\varepsilon_2)e^{2n\alpha_1}+(\varepsilon_1+\varepsilon_2)e^{2n\alpha_2}]^2}. \tag{12}$$

Since the problem is invariant to the rotation of the particle about its axis, the torque must be equal to zero. The potential can always be decomposed to a sum of symmetric and antisymmetric components. Since the dielectric forces are insensitive to the sign of the polarization charge, there cannot be a net force in the y direction $(F_y=0)$. In the next section, we will reproduce these latter results explicitly.

B. Force calculation based on the Maxwell tensor

Alternatively, the force can be calculated from the Maxwell stress tensor:[12]

$$\mathbf{T}=\varepsilon_0\varepsilon_1\left(\mathbf{EE}-\frac{1}{2}(\mathbf{E}\cdot\mathbf{E})\mathbf{I}\right), \tag{13}$$

where $\mathbf{I}$ is the unit tensor. The DEP force is obtained by integrating $\mathbf{T}$ over any closed surface (S_i) that surrounds the particle:

$$\mathbf{F}=\oint_{S_i}(\mathbf{T}\cdot\mathbf{n})dS_i. \tag{14}$$

On the surface of the particle, $\mathbf{n}=-\mathbf{e}_\alpha$. The surface force densities in the α and β directions are, respectively,

$$f_\alpha=\frac{\varepsilon_0\varepsilon_1}{2h^2}\left[\left(\frac{\partial\phi_1}{\partial\alpha}\right)^2-\left(\frac{\partial\phi_1}{\partial\beta}\right)^2\right] \tag{15}$$

and

$$f_\beta=\frac{\varepsilon_0\varepsilon_1}{h^2}\left(\frac{\partial\phi_1}{\partial\alpha}\right)\left(\frac{\partial\phi_1}{\partial\beta}\right). \tag{16}$$

The electrostatic forces per unit length in the x and y directions are, respectively,

$$F_x=-\int_{-\pi}^{\pi}(f_\alpha\cos\theta+f_\beta\sin\theta)hd\beta \tag{17}$$

and

$$F_y = \int_{-\pi}^{\pi} (f_\beta \cos\theta - f_\alpha \sin\theta) h d\beta. \tag{18}$$

In the above,

$$h = \frac{a}{\cosh\alpha - \cos\beta} \tag{19}$$

is the scale factor, and θ is the angle between the unit vector $\mathbf{e}_\alpha$ and the x direction. $\sin\theta = y/r_2$ and $\cos\theta = (x - a\coth\alpha)/r_2$. Not surprisingly, upon integrating Eq. (17), we obtain Eq. (12), and Eq. (18) yields $F_y = 0$.

C. Conducting particles

The DEP forces that act on electrically conductive particles can be obtained from the expressions derived earlier in the limit of $\varepsilon_2/\varepsilon_1 \to \infty$. Alternatively, the potential field can be calculated directly by taking into consideration the fact that the potential of the particle is uniform and the particle is electrically neutral. In other words, on the surface of the particle, we have $\phi_2 = V =$ constant and

$$\int_{S_2} \varepsilon_0 \varepsilon_1 \nabla \phi_1 \cdot \mathbf{n} dS_2 = 0. \tag{20}$$

The corresponding solution of the Laplace equation for the potential is

$$\phi_1 = \sum_{n=1}^{\infty} \frac{\sinh n(\alpha - \alpha_2)}{\sinh n(\alpha_1 - \alpha_2)} [a_n \sin n\beta + b_n \cos n\beta] + V \frac{\alpha - \alpha_1}{\alpha_2 - \alpha_1}, \tag{21}$$

where $V = 0$. The x-direction force per unit length on the particle calculated from the Maxwell stress tensor is

$$F_x = -\frac{\pi \varepsilon_0 \varepsilon_1}{2a} \sum_{n=1}^{\infty} \frac{n^2 (a_n^2 + b_n^2)}{\sinh^2 n(\alpha_1 - \alpha_2)}. \tag{22}$$

D. Force calculation based on the effective dipole-moment approximation

One of our objectives is to compare the frequently used dipole-moment approximation with the more accurate (and tedious) calculation of the force presented in the previous sections. According to the dipole-moment approximation, the DEP force acting on the particle is[2]

$$\mathbf{F} = \mathbf{p}_{\text{eff}} \cdot \nabla \mathbf{E}_{0,c} = \pi r_2^2 \varepsilon_0 \varepsilon_1 \frac{\varepsilon_2 - \varepsilon_1}{\varepsilon_1 + \varepsilon_2} (\nabla(\mathbf{E} \cdot \mathbf{E}))_{0,c}, \tag{23}$$

where the dipole moment $\mathbf{p}_{\text{eff}}$ is defined as the moment of an equivalent line dipole that produces the same electrostatic potential when immersed in the same dielectric liquid and positioned at the location of the center of the particle. In the above, $\alpha_c = 2\alpha_2$ and $\beta_c = 0$ are the bicylindrical coordinates of the center of the particle. The dipole moment for the planar cylindrical particle is $\mathbf{p}_{\text{eff}} = 2\pi\varepsilon_1(\varepsilon_2 - \varepsilon_1)/(\varepsilon_1 + \varepsilon_2) r_2^2 \mathbf{E}_c$.[15]

The electric field in the absence of the particle is

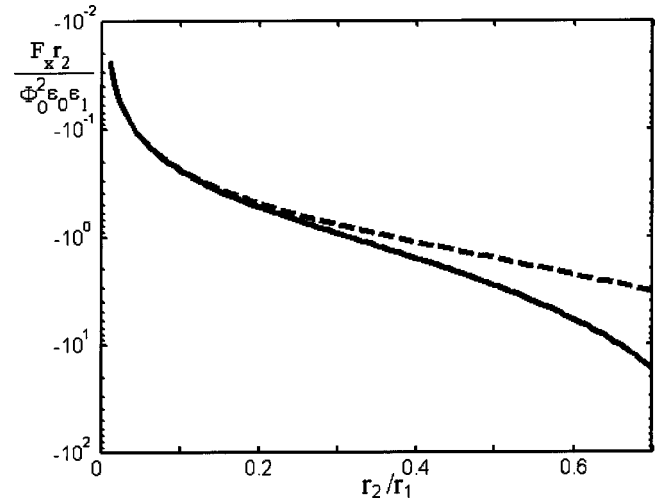

FIG. 3. The normalized exact (solid line) and approximate (dashed line) x-direction DEP forces acting on a cylindrical particle submerged in a cylindrical shell as functions of r_2/r_1 when $c/r_1 = 0.2$ $\varepsilon_2/\varepsilon_1 = 10$, and the potential of the outer shell $\phi = \Phi_0 \sin\beta$.

$$\mathbf{E}_0 = \frac{1}{h} \sum_{n=1}^{\infty} n e^{n(\alpha_1 - \alpha)} [(a_n \sin(n\beta) + b_n \cos(n\beta)) \mathbf{e}_\alpha - (a_n \cos(n\beta) - b_n \sin(n\beta)) \mathbf{e}_\beta]. \tag{24}$$

The x, y components of the DEP force are

$$F_x = \frac{8\pi\varepsilon_0\varepsilon_1(\varepsilon_2 - \varepsilon_1)\sinh^2\alpha_2}{r_2(\varepsilon_1 + \varepsilon_2)} \times \sum_{n=1}^{\infty} \sum_{m=1}^{\infty} nm(a_n a_m + b_n b_m) e^{(n+m)(\alpha_1 - 2\alpha_2)} \times [(n+m)\sinh\alpha_2 - 2\cosh\alpha_2] \tag{25}$$

and

$$F_y = \frac{8\pi\varepsilon_0\varepsilon_1(\varepsilon_1 - \varepsilon_2)\sinh^3\alpha_2}{r_2(\varepsilon_1 + \varepsilon_2)} \sum_{n=1}^{\infty} \sum_{m=1}^{\infty} nm(n-m) \times (a_m b_n - a_n b_m) e^{(n+m)(\alpha_1 - 2\alpha_2)}. \tag{26}$$

For certain distributions of the surface potential, the dipole-moment approximation predicts a nonzero force in the y direction. No such force exists, however.

E. The range of validity of the dipole-moment approximation

To estimate the range of validity of the dipole-moment approximation, we compare the force estimates of the dipole-moment approximation with the exact values in the special case of a semi-infinite medium and surface potential $f(\beta) = \Phi_0 \sin(\beta)$. Figure 3 depicts the exact [solid line, Eq. (12)] and approximate [dashed line, Eq. (25)] x-direction normalized DEP forces as functions of r_2/r_1 when $c/r_1 = 0.2$ and $\varepsilon_2/\varepsilon_1 = 10$. The force per unit length of the particle was normalized with $\Phi_0^2 \varepsilon_0 \varepsilon_1 / r_2$. In this particular example, the radius of the shell r_1 represents the length scale of the electric field. When the radii ratio (r_2/r_1) is small, the presence

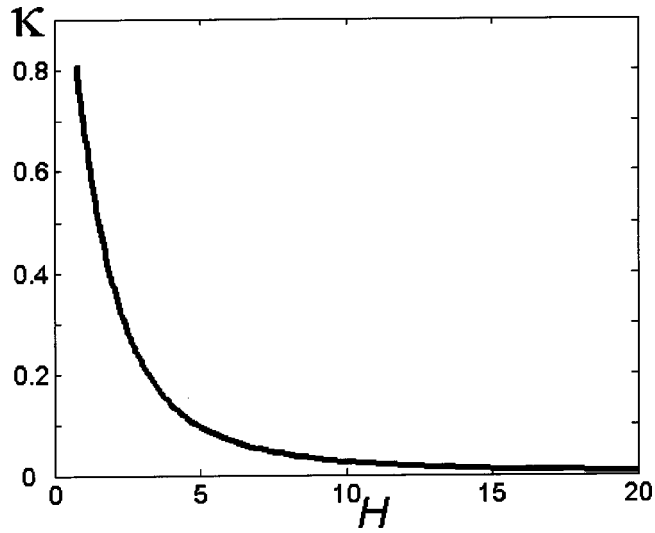

FIG. 4. The relative difference (κ) between the exact and approximate values of the x-direction DEP force on the cylindrical particle as a function of H for the same conditions as in Fig. 3.

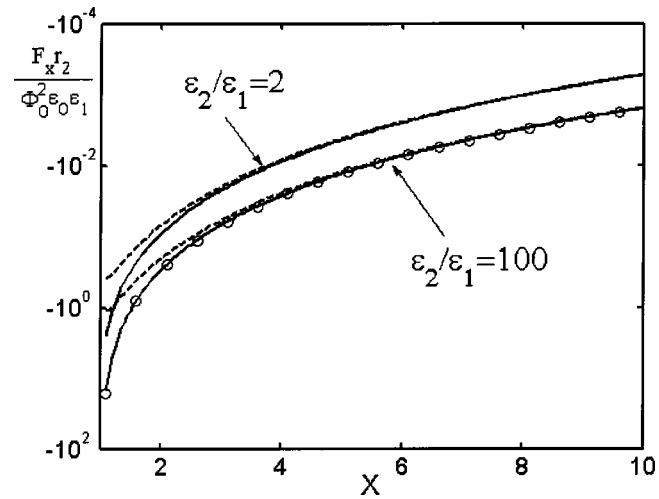

FIG. 5. The exact (solid lines) and approximate (dashed lines), dimensionless electrostatic forces acting on a cylindrical particle embedded in a semi-infinite medium as functions of the dimensionless distance from the center of the particle to the plane (X) when $\varepsilon_2/\varepsilon_1=2$ and $\varepsilon_2/\varepsilon_1=100$.

of the cylindrical particle introduces only a small disturbance in the electric field and the dipole-moment calculation provides an excellent approximation. When the radii ratio is larger than 0.2, the dipole-moment approximation deviates considerably from the exact value.

In general, it is more convenient to use H as the measure of the length scale of the electric field relative to the size of the particle. Figure 4 depicts the relative difference κ between the exact and the dipole-moment calculation of the x component of the DEP force as a function of H for the same conditions as in Fig. 3. When $H>10$, the dipole moment approximation is accurate within better than 3%. More disturbingly, the dipole-moment approximation predicts a force in the y direction when none exists.

F. A particle in a semi-infinite medium with surface potential $f(\beta)=\Phi_0 \sin(\beta)$

In this section, we consider a semi-infinite medium with the surface potential $f(\beta)=\Phi_0 \sin(\beta)$ at $(\alpha=\alpha_1=0)$. This potential distribution is a crude approximation of the potential used in our experimental setup, where we maintain a potential difference across two electrodes with a gap between them. In Cartesian coordinates, $\cos(\beta)=[\sqrt{(x^2+y^2-a^2)^2}/\sqrt{a^4-2a^2(x^2-y^2)+(x^2+y^2)^2}]$.

The distance of the center of the cylinder from the wall is denoted as d (see Fig. 1), $a=\sqrt{d^2-r_2^2}$, and $\alpha_2=\ln[(d+\sqrt{d^2-r_2^2})/r_2]$. The x-direction DEP force reduces to

$$F_{x,\text{exact}}=\frac{\pi\varepsilon_0\varepsilon_1(\varepsilon_1^2-\varepsilon_2^2)r_2^2(2d^2-r_2^2+2d\sqrt{d^2-r_2^2})\Phi_0^2}{2\sqrt{d^2-r_2^2}[(\varepsilon_1+\varepsilon_2)(d^2+d\sqrt{d^2-r_2^2})-\varepsilon_2 r_2^2]^2}. \tag{27}$$

The corresponding dipole-moment approximation gives

$$F_{x,\text{DM}}=\frac{16\pi\varepsilon_0\varepsilon_1(\varepsilon_2-\varepsilon_1)r_2^2(d^2-r_2^2)\Phi_0^2}{(\varepsilon_1+\varepsilon_2)(d+\sqrt{d^2-r_2^2})^5} \tag{28}$$

and $F_y=0$. When the cylinder is conducting, the exact force expression simplifies to

$$F_x=-\frac{\varepsilon_1\varepsilon_0\pi\Phi_0^2 r_2^2}{2(d^2-r_2^2)^{3/2}}. \tag{29}$$

In the limit of $r_2\to 0$, the exact force and dipole-moment approximation can be expanded into the corresponding Taylor series in terms of r_2

$$F_{x,\text{exact}}\sim \pi r_2^2\frac{\varepsilon_0\varepsilon_1(\varepsilon_1-\varepsilon_2)}{2(\varepsilon_1+\varepsilon_2)d^3}\Phi_0^2 + \pi r_2^4\frac{\varepsilon_0\varepsilon_1(\varepsilon_1-\varepsilon_2)(\varepsilon_1+3\varepsilon_2)}{4(\varepsilon_1+\varepsilon_2)^2 d^5}\Phi_0^2+O(d^{-7}) \tag{30}$$

and

$$F_{x,\text{DM}}\sim \pi r_2^2\frac{\varepsilon_0\varepsilon_1(\varepsilon_1-\varepsilon_2)}{2(\varepsilon_1+\varepsilon_2)d^3}\Phi_0^2+\pi r_2^4\frac{\varepsilon_0\varepsilon_1(\varepsilon_1-\varepsilon_2)}{8(\varepsilon_1+\varepsilon_2)d^5}\Phi_0^2 + O(d^{-7}). \tag{31}$$

Witness that the leading-order terms are identical in both cases. The second-order terms are different, however.

When the particle is far from the wall, the dielectrophoretic force scales like $O(d^{-3})$. When the particle is close to the wall $(d-r_2\ll r_2)$ and $\varepsilon_2\ll\infty$, we have

$$F_{x,\text{exact}}\sim -\sqrt{\frac{2}{r_2}}\frac{\pi\varepsilon_0(\varepsilon_2^2-\varepsilon_1^2)\Phi_0^2}{4\varepsilon_1}(d-r_2)^{-1/2} + \frac{\pi\varepsilon_0\varepsilon_2(\varepsilon_2^2-\varepsilon_1^2)\Phi_0^2}{\varepsilon_1^2 r_2}+O((d-r_2)^{1/2}). \tag{32}$$

In other words, the dielectrophoretic force scales like $\delta^{-1/2}$, where $\delta=d-r_2$. The singularity depends on potential distribution on the surface and on the dielectric properties of the particle. When the particle is conducting, the singularity is even stronger.

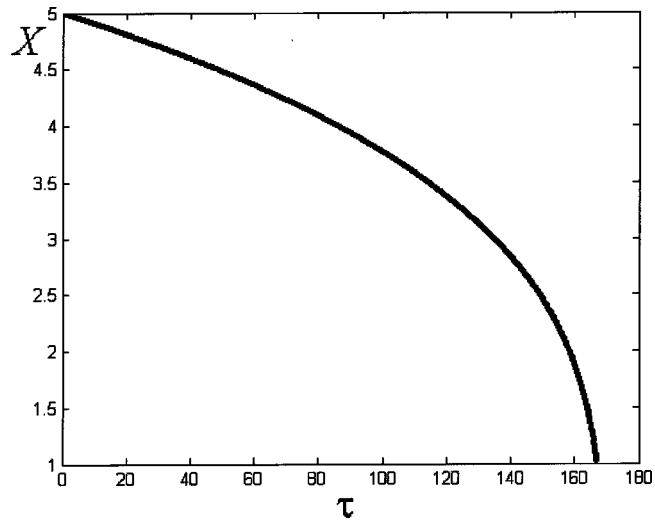

FIG. 6. The dimensionless distance X of the center of the cylindrical particle from the plane as a function of the dimensionless time when $X(0)=5$, $\varepsilon_2/\varepsilon_1=10$, and the surface potential is $\phi=\Phi_0 \sin\beta$.

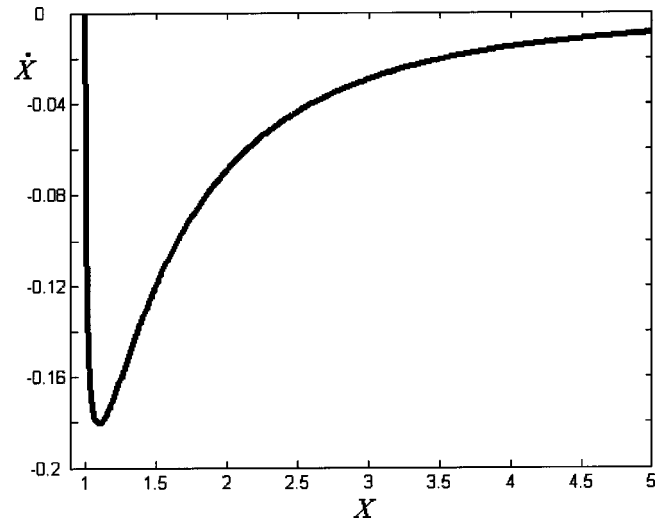

FIG. 7. The dimensionless velocity $\dot{X}$ of the cylindrical particle as a function of its distance X from the plane when $X(0)=5$, $\varepsilon_2/\varepsilon_1=10$, and the surface potential is $\phi=\Phi_0 \sin\beta$.

G. The migration of a particle in a semi-infinite viscous medium

Next, we consider a cylindrical particle embedded in a semi-infinite, viscous (with viscosity μ), perfectly dielectric medium. A nonuniform potential is specified on the surface of the medium. Figure 5 depicts the dimensionless electrostatic force acting on the particle as a function of its dimensionless distance ($X=d/r_2$) from the plane when $\varepsilon_2/\varepsilon_1=2$ and $\varepsilon_2/\varepsilon_1=100$. The solid and dashed lines in Fig. 5 correspond, respectively, to the exact force and the dipole-moment approximation. Since $\varepsilon_2>\varepsilon_1$, the force is directed toward the wall (positive dielectrophoresis). As the particle approaches the surface, the magnitude of the force increases rapidly.

The electrostatic force causes the particle to migrate. Since typically the resulting motion is quite slow, we assume that inertial effects can be neglected and the fluid motion can be described with the Stokes equation. The instantaneous distance of the center of the particle from the wall is denoted as X (see Fig. 1), and the instantaneous velocity of the particle in the x direction is denoted $\dot{X}$, where the superscript dot indicates a time derivative. Since there are no forces in the y direction, the motion is confined to the x axis ($y=0$).

For concreteness, we consider the case of $f(\beta)=\Phi_0 \sin\beta$. The x direction DEP force is given in Eq. (27). Jeffery and Onishi[16] computed the expressions for the drag force on the cylinder translating perpendicular to a plane,

$$D_x=\frac{-4\pi\mu\dot{d}}{\alpha_2-\tanh\alpha_2}=\frac{-4\pi\mu\dot{d}}{\ln[(d+\sqrt{d^2-r_2^2})/r_2]-\sqrt{d^2-r_2^2}/d}. \tag{33}$$

When inertia is negligible; the DEP force is balanced by the viscous drag. Equating the electrostatic and viscous forces, we obtain a first-order differential equation for the instantaneous velocity,

$$\frac{dX}{d\tau}=\frac{(\varepsilon_1^2-\varepsilon_2^2)(X+\sqrt{X^2-1})^2[\ln(X+\sqrt{X^2-1})-\sqrt{1-X^{-2}}]}{\sqrt{X^2-1}[(\varepsilon_1+\varepsilon_2)X(X+\sqrt{X^2-1})-\varepsilon_2]^2}, \tag{34}$$

with the initial condition $X(0)=X_0$, where X_0 is the position of the particle at time $t=0$. τ is the dimensionless time. In the above, we use $8\mu r_2^2/(\Phi_0^2\varepsilon_0\varepsilon_1)$ as the time scale.

We integrated Eq. (34) numerically using a fourth-order Runge–Kutta algorithm. Figure 6 depicts X as a function of the dimensionless time (τ) when $X(0)=5$. Figure 7 depicts the dimensionless velocity $\dot{X}$ as a function of the particle's position X. Witness that as the particle approaches the wall, the absolute value of the velocity increases, achieves a maximum, and then decreases to zero. The dimensionless total migration time depends on the initial position of the particle and the dielectric constants of the particle and the suspending medium.

When the particle is far from the wall ($d/r_2\to\infty$), the viscous drag scales like

$$D_x\sim\pi\mu\dot{d}\left(\frac{4}{1-\ln(2d/r_2)}+\frac{r_2^2}{d^2(1-\ln(2d/r_2))^2}\right)+O(d^{-4}), \tag{35}$$

and the particle velocity is on the order of $d^3\ln(d)$.

When the particle is close to the wall ($d-r_2\ll r_2$),

$$D_x \sim -\sqrt{2}\pi\mu\dot{d}(3r_2^{3/2}(d-r_2)^{-3/2} + 21/20 r_2^{1/2}(d-r_2)^{-1/2}) + O((d-r_2)^{1/2}), \quad (36)$$

and the velocity of the particle scales like $(d-r_2)$. In other words, when the particle is close to the surface, its velocity is proportional to the gap size between the particle and the surface.

IV. SPHERICAL PARTICLE EMBEDDED IN A SPHERICAL SHELL

We consider a sphere of radius r_2 and relative dielectric permittivity ε_2 submerged in a second sphere of radius r_1. The distance between the centers of the two spheres is c. The domain between the spheres is filled with a dielectric, viscous fluid with permittivity ε_1 and viscosity μ.

It is convenient to use bispherical coordinates.[13] The relationships between the bispherical and Cartesian coordinates are given below:

$$\begin{aligned} x &= a \sin\alpha/(\cosh\alpha - \cos\beta), \\ y &= a \sin\beta \cos\gamma/(\cosh\alpha - \cos\beta), \\ z &= a \sin\beta \sin\gamma/(\cosh\alpha - \cos\beta), \end{aligned} \quad \begin{pmatrix} -\infty < \alpha < \infty \\ 0 \leqslant \beta \leqslant \pi \\ 0 \leqslant \gamma \leqslant 2\pi \end{pmatrix}. \quad (37)$$

Surfaces of constant α correspond to spheres of radius $a/\sinh\alpha$:

$$(x - a\coth\alpha)^2 + y^2 + z^2 = a^2/\sinh^2\alpha. \quad (38)$$

The surfaces of the outer and inner spheres correspond, respectively, to $\alpha=\alpha_1$ and $\alpha=\alpha_2$ $(\alpha_1 \leqslant \alpha \leqslant \alpha_2)$. Constant β coordinates represent a second family of spheres that are orthogonal to the constant α surfaces. γ represents the angular direction.

The Laplace equation for the electrical potential in the bispherical coordinates has the form

$$\nabla^2\phi = \frac{(\cosh\alpha - \cos\beta)^2}{a^2 \sin\beta}\left[\sin\beta \frac{\partial}{\partial\alpha}\left(\frac{1}{\cosh\alpha - \cos\beta}\frac{\partial\phi}{\partial\alpha}\right) + \frac{\partial}{\partial\beta}\left(\frac{\sin\beta}{\cosh\alpha - \cos\beta}\frac{\partial\phi}{\partial\beta}\right) + \frac{1}{\sin\beta(\cosh\alpha - \cos\beta)}\frac{\partial^2\phi}{\partial\gamma^2}\right] = 0. \quad (39)$$

The Laplace equation admits a general solution of the form[17]

$$\phi = \sqrt{\cosh\alpha - \cos\beta} \times \sum_{n=0}^{\infty}\sum_{m=-n}^{n}(A_n e^{(n+1/2)\alpha} + B_n e^{-(n+1/2)\alpha}) \times (A_n' \sin m\gamma + B_n' \cos m\gamma) P_n^m(\cos\beta), \quad (40)$$

where P_n^m is the associated Legendre function of the first kind. The associated Legendre function of the second kind, Q_n^m, does not appear because it diverges at $\beta=\pi/2$. As we shall shortly see, the presence of the factor $\sqrt{\cosh\alpha - \cos\beta}$ in (40) precludes us from obtaining explicit expressions for the Fourier coefficients in the series. To simplify matters, we will focus only on the case of a spherical particle embedded in a semi-infinite medium $(\alpha_1=0)$. This case is of interest for particle trapping.

A. The potential field in the axisymmetric case (ϕ is independent of γ)

When the electrical potential has cylindrical symmetry about the x axis, $m=0$ and the electrical potentials in domains 1 and 2 are, respectively,

$$\phi_1 = \sqrt{\cosh\alpha - \cos\beta} \times \sum_{n=0}^{\infty}(A_n e^{(n+1/2)\alpha} + B_n e^{-(n+1/2)\alpha}) P_n(\cos\beta) \quad (41)$$

and

$$\phi_2 = \sqrt{\cosh\alpha - \cos\beta}\sum_{n=0}^{\infty} C_n e^{-(n+1/2)\alpha} P_n(\cos\beta). \quad (42)$$

The boundary condition at $\alpha=0$ is

$$\phi_1 = f(\cos\beta)\sqrt{1-\cos\beta}, \quad (43)$$

where $f(\cos\beta)=\Sigma_{n=0}^{\infty} F_n P_n(\cos\beta)$ and $F_n=(2n+1)/n \int_{-1}^{1} f(t)P_n(t)dt$. When we apply the interfacial boundary conditions [Eqs. (3) and (4)] at $\alpha=\alpha_2$, we obtain an infinite set of recurrence equations for the coefficients A_n:

$$e^{-\alpha_2}(n+1)u_{n+1}A_{n+1} + e^{\alpha_2} n u_{n-1} A_{n-1} + \nu_n A_n = M_n, \quad (n=1,2,\ldots), \quad (44)$$

where $u_n=(\varepsilon_2/\varepsilon_1 - 1)e^{(2n+1)\alpha_1} - (\varepsilon_2/\varepsilon_1 + 1)e^{(2n+1)\alpha_2}$, $\nu_n = 2\sinh\alpha_2 e^{(2n+1)\alpha_2} - (e^{-\alpha_2} + 2n\cosh\alpha_2)u_n$, and $M_n = (1-\varepsilon_2/\varepsilon_1)[e^{(n+1/2)\alpha_1}(e^{-\alpha_2} + 2n\cosh\alpha_2)F_n - (n+1)e^{(n+3/2)\alpha_1 - \alpha_2}F_{n+1} - n e^{(n-1/2)\alpha_1 + \alpha_2}F_{n-1}]$. For additional details of the derivation of Eq. (44), see, among other places, Bau.[18]

The above set of equations cannot be solved in a closed form since any N equations involve $(N+1)$ unknowns. Assuming that the surface potential obeys certain regularity conditions, series (41) will converge, and A_n will form a decaying sequence. Hence, we truncate the equations at some $n=N$. By setting $A_{N+1}=0$, we solve (44). When the particle is far from the surface, the rate of convergence is rapid and only a few terms in the series are needed to obtain accurate solutions. For example, $A_0 = -9.449\times10^{-5}$, $A_3 = 5.524\times10^{-10}$, and $A_5 = 3.339\times10^{-15}$ when $d/r_2=10$, and $\varepsilon_2/\varepsilon_1=10$. The rate of convergence deteriorates as the distance between the center of the particle and the plane decreases.

Once A_n has been calculated, the coefficients B_n and C_n are readily determined from

$$B_n = F_n e^{(n+1/2)\alpha_1} - A_n e^{(2n+1)\alpha_1} \quad (45)$$

and

$$C_n = F_n e^{(n+1/2)\alpha_1} + A_n \lfloor e^{(2n+1)\alpha_2} - e^{(2n+1)\alpha_1} \rfloor. \quad (46)$$

B. The potential field in the asymmetric case (ϕ dependence on γ)

To simplify matters, we consider only the case when the surface potential varies like $\sin(\gamma)$. In other words, $m=1$ in Eq. (40). Higher modes can be treated in an analogous manner. The potentials are

$$\phi_1=\sqrt{\cosh\alpha-\cos\beta}\sum_{n=1}^{\infty}(D_n e^{(n+1/2)\alpha}+E_n e^{-(n+1/2)\alpha})P_n^1(\cos\beta)\sin\gamma \tag{47}$$

and

$$\phi_2=\sqrt{\cosh\alpha-\cos\beta}\sum_{n=1}^{\infty}H_n e^{-(n+1/2)\alpha}P_n^1(\cos\beta)\sin\gamma \tag{48}$$

with the boundary condition at $\alpha=\mathbf{0}$:

$$\phi_1=g(\cos\beta)\sqrt{1-\cos\beta}\sin\gamma, \tag{49}$$

where $g(\cos\beta)=\Sigma_{n=1}^{\infty}G_nP_n^1(\cos\beta)$ and $G_n=(2n+1)/2/n/(n+1)\int_{-1}^{1}g(t)P_n^1(t)dt$. The coefficients D_n, E_n, and H_n satisfy

$$e^{-\alpha_2}(n+1)u_{n+1}D_{n+1}+e^{\alpha_2}nu_{n-1}D_{n-1}+\nu_nD_n=Z_n,\quad (n=1,2,.....), \tag{50}$$

$$E_n=G_ne^{(n+1/2)\alpha_1}-D_ne^{(2n+1)\alpha_1}, \tag{51}$$

and

$$H_n=G_ne^{(n+1/2)\alpha_1}+D_n[e^{(2n+1)\alpha_2}-e^{(2n+1)\alpha_1}], \tag{52}$$

where $Z_n=(1-\varepsilon_2/\varepsilon_1)[e^{(n+1/2)\alpha_1}(e^{-\alpha_2}+2n\cosh\alpha_2)G_n-(n+1)e^{(n+3/2)\alpha_1-\alpha_2}G_{n+1}-ne^{(n-1/2)\alpha_1+\alpha_2}G_{n-1}]$ and $D_0=0$.

C. Dielectrophoretic force in the axisymmetric case (ϕ is independent of γ)

The calculation of the dielectrophoretic forces proceeds along similar lines as in the planar case. As before, we denote the distance between the center of the sphere and the wall as d. $a=\sqrt{d^2-r_2^2}$ and $\alpha_2=\ln[(d+\sqrt{d^2-r_2^2})/r_2]$. It is convenient to carry out the necessary integrations on the planar surface ($\alpha=0$) rather than on the surface of the particle. On the plane ($\alpha=0$), we have $\mathbf{e}_\alpha=\mathbf{e}_x$.

In the axisymmetric case, the x-direction force is given by the integral:

$$F_x=\varepsilon_0\varepsilon_1\int_0^{2\pi}\int_0^{\pi}\frac{\sin\beta}{2}\left[\left(\frac{\partial\phi_1}{\partial\beta}\right)^2-\left(\frac{\partial\phi_1}{\partial\alpha}\right)^2\right]_{\alpha=0}d\beta d\gamma. \tag{53}$$

Due to symmetry, the other two force components and the torque are identically equal to zero. In other words,

$$F_y=\varepsilon_0\varepsilon_1\int_0^{2\pi}\int_0^{\pi}\sin\beta\left[\frac{\partial\phi_1}{\partial\alpha}\frac{\partial\phi_1}{\partial\beta}\right]_{\alpha=0}\sin\gamma d\beta d\gamma=0. \tag{54}$$

Likewise,

$$F_z=\varepsilon_0\varepsilon_1\int_0^{2\pi}\int_0^{\pi}\sin\beta\left[\frac{\partial\phi_1}{\partial\alpha}\frac{\partial\phi_1}{\partial\beta}\right]_{\alpha=0}\cos\gamma d\beta d\gamma=0. \tag{55}$$

Next, we obtain explicit expressions for the x-direction force in the special case of $f(\cos\beta)=\Phi_0$:

$$F_x=-2\pi\varepsilon_0\varepsilon_1\Phi_0^2\left[A_0^2-A_0(1+2A_1)+A_1(1+3A_1-2A_2)+4\sum_{n=2}^{\infty}A_n[(2n+1)A_n-(n+1)A_{n+1}-nA_{n-1}]\right]. \tag{56}$$

The effective dipole moment of a dielectric sphere is[2]

$$\mathbf{p}_{\text{eff}}=4\pi\varepsilon_1\varepsilon_0\frac{\varepsilon_2-\varepsilon_1}{\varepsilon_2+2\varepsilon_1}r_2^3\mathbf{E}_{0,c}, \tag{57}$$

where $\mathbf{E}_{0,c}$ is the electric field at the location of the center of the sphere in its absence. The potential field in the absence of the sphere is

$$\phi_0=\sqrt{\cosh\alpha-\cos\beta}\sum_{n=0}^{\infty}F_ne^{-(n+1/2)\alpha}P_n(\cos\beta). \tag{58}$$

Applying boundary condition $f(\cos\beta)=\Phi_0$ yields

$$\phi_0=\Phi_0\sqrt{\cosh\alpha-\cos\beta}e^{-1/2\alpha}. \tag{59}$$

Therefore, the x-direction dipole-moment approximation of the DEP force is

$$F_x=\frac{16\pi\varepsilon_0\varepsilon_1(\varepsilon_1-\varepsilon_2)\Phi_0^2r_2^3(d^2-r_2^2)}{(\varepsilon_2+2\varepsilon_1)(d+\sqrt{d^2-r_2^2})^5}. \tag{60}$$

For the particular surface potential distribution used here, the dipole-moment approximation predicts zero DEP forces in the y and z directions.

D. Dielectrophoretic force in the asymmetric case (ϕ is a function of γ)

The expression for the electrostatic force in the x direction is

$$F_x=\varepsilon_0\varepsilon_1\int_0^{2\pi}\int_0^{\pi}\frac{\sin\beta}{2}\left[\left(\frac{\partial\phi_1}{\partial\beta}\right)^2-\left(\frac{\partial\phi_1}{\partial\alpha}\right)^2+\frac{1}{\sin^2\beta}\left(\frac{\partial\phi_1}{\partial\gamma}\right)^2\right]_{\alpha=0}d\beta d\gamma. \tag{61}$$

The expressions for the y- and z-direction forces and the torque are

$$F_y=\varepsilon_0\varepsilon_1\int_0^{2\pi}\int_0^{\pi}\left\{\sin\beta\left[\frac{\partial\phi_1}{\partial\alpha}\frac{\partial\phi_1}{\partial\beta}\right]_{\alpha=0}\sin\gamma+\left[\frac{\partial\phi_1}{\partial\alpha}\frac{\partial\phi_1}{\partial\gamma}\right]_{\alpha=0}\cos\gamma\right\}d\beta d\gamma, \tag{62}$$

$$F_z=\varepsilon_0\varepsilon_1\int_0^{2\pi}\int_0^{\pi}\left\{\sin\beta\left[\frac{\partial\phi_1}{\partial\alpha}\frac{\partial\phi_1}{\partial\beta}\right]_{\alpha=0}\cos\gamma-\left[\frac{\partial\phi_1}{\partial\alpha}\frac{\partial\phi_1}{\partial\gamma}\right]_{\alpha=0}\sin\gamma\right\}d\beta d\gamma, \tag{63}$$

and

$$T_x=\varepsilon_0\varepsilon_1\int_0^{2\pi}\int_0^{\pi}\left[\frac{\partial\phi_1}{\partial\alpha}\frac{\partial\phi_1}{\partial\gamma}\right]_{\alpha=0}\sqrt{y^2+z^2}d\beta d\gamma. \tag{64}$$

Expressions (62) and (63) contain integrals of the form,

$$\int_0^{2\pi}\begin{pmatrix}\sin^2 n\gamma\\ \cos^2 n\gamma\\ \sin n\gamma\cos n\gamma\end{pmatrix}\begin{pmatrix}\sin\gamma\\ \cos\gamma\end{pmatrix}d\gamma, \tag{65}$$

where n is an integer. Not surprisingly, all these integrals are identically equal to zero. Hence, we conclude that for any continuous surface potential distribution, $F_y=F_z=0$. Based on symmetry, we argue that also $T_x=0$.

Next, we calculate the x-direction force for the special case of $g(\cos\beta)=\Phi_0P_1^1(\cos\beta)=\Phi_0\sqrt{1-\cos^2\beta}$. Upon substituting Eqs. (47) and (50) into (61) and applying the boundary condition, we have

$$F_x=\Phi_0^2\frac{\pi\varepsilon_1\varepsilon_0}{2}\left[3-3(2D_1-1)(2D_1-4D_2-1)-\sum_{n=2}^{\infty}2n(n+1)D_n[(2n+1)D_n-(2n+4)D_{n+1}]\right]. \tag{66}$$

Finally, we use the dipole-moment approximation to calculate the forces. The electric potential in the absence of the sphere is

$$\phi_0=\sqrt{\cosh\alpha-\cos\beta}\sum_{n=1}^{\infty}G_ne^{-(n+1/2)\alpha}P_n^1(\cos\beta)\sin\gamma. \tag{67}$$

Applying boundary condition $g(\cos\beta)=\Phi_0\sqrt{1-\cos^2\beta}$ yields

$$\phi_0=\Phi_0\sqrt{\cosh\alpha-\cos\beta}\sqrt{1-\cos^2\beta}e^{-3/2\,\alpha}\sin\gamma. \tag{68}$$

Therefore, the x-direction dipole-moment approximation for the DEP force is

$$F_x=\frac{96\pi\varepsilon_1\varepsilon_0\Phi_0^2(\varepsilon_2-\varepsilon_1)\sinh^4\alpha_2(\cosh 7\alpha_2-\sinh 7\alpha_2)}{(\varepsilon_2+2\varepsilon_1)}. \tag{69}$$

For the particular surface potential distribution used here, the dipole-moment approximation predicts $F_y=F_z=T_x=0$.

E. The range of validity of the dipole-moment approximation

In this section, we compare the exact values of the force with the predictions of the dipole-moment approximation. Figure 8 depicts the normalized x-direction exact (solid line) and approximate (dashed line) DEP forces ($F_x^*=F_x/\varepsilon_1\varepsilon_0\Phi_0^2$) as functions of the normalized distance X $(=d/r_2)$ from the plane when $\varepsilon_2/\varepsilon_1=10$ and $\phi=\Phi_0\sqrt{1-\cos\beta}$ on the plane. We also calculated the forces using finite elements (FEMLAB).[19] The finite element calculations are shown as solid circles in Fig. 8 and are in excellent agreement with the exact solution. Witness that the dipole-moment approximation works well when $X>5$. When $X=1.2$, 5, and 10, the relative differences between the dipole moment approximation and the exact solution are, respectively, 63.3%, 2.0%, and 0.4%.

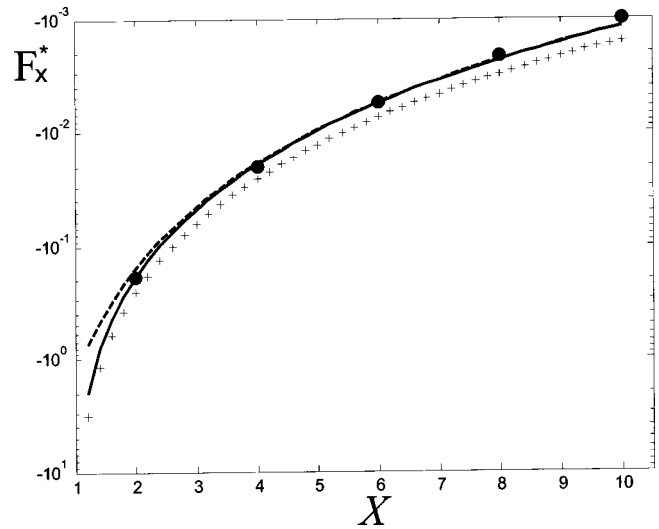

FIG. 8. The normalized x-direction exact (solid line) and approximate (dashed line) DEP forces F_x^* acting on a spherical particle as functions of the normalized distance X from the plane when $\varepsilon_2/\varepsilon_1=10$ and the surface potential is $\phi=\Phi_0\sqrt{1-\cos\beta}$. The solid circles correspond to finite element calculations ($\varepsilon_2/\varepsilon_1=10$). The symbols + correspond to an exact force for a conducting sphere.

Our results are consistent with the results of other researchers. For example, Tao *et al.*[20] used finite elements to calculate the interparticle forces in a chain of uniformly spaced particles. They found the dipole-moment approximation to grossly underestimate the dielectrophoretic forces when the ratio between the dielectric constants of the particle and the surrounding medium was large and when the relative distances between the particles were small. These circumstances correspond to the length scale associated with the electric field being relatively small compared to the size of the particle (small values of our dimensionless parameter H).

To further explore the range of validity of the dipole-moment approximation, we depict in Fig. 9 the relative difference between the exact force value and the dipole moment approximation as a function of H. When $H>2$, the relative error is within 3%.

It is interesting to compare the Taylor series expansions of the exact expression for the force and the dipole-moment approximation. In the limit $d/r_2\to\infty$,

$$F_{x,\text{exact}}\sim\frac{3\varepsilon_0\varepsilon_1(\varepsilon_1-\varepsilon_2)\pi\Phi_0^2}{8(2\varepsilon_1+\varepsilon_2)}\left[\frac{4r_2^3}{3d^3}+\frac{r_2^5}{d^5}\right]+O(d^{-7}) \tag{70}$$

and

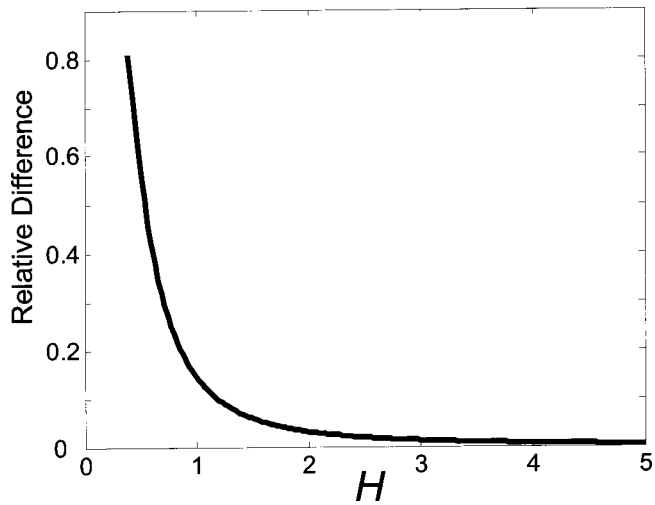

FIG. 9. The relative difference between the exact and the dipole moment approximation of the x-direction DEP force acting on a spherical particle as a function of H when $\varepsilon_2/\varepsilon_1=10$ and the potential of the plane is $\phi=\Phi_0\sqrt{1-\cos\beta}$.

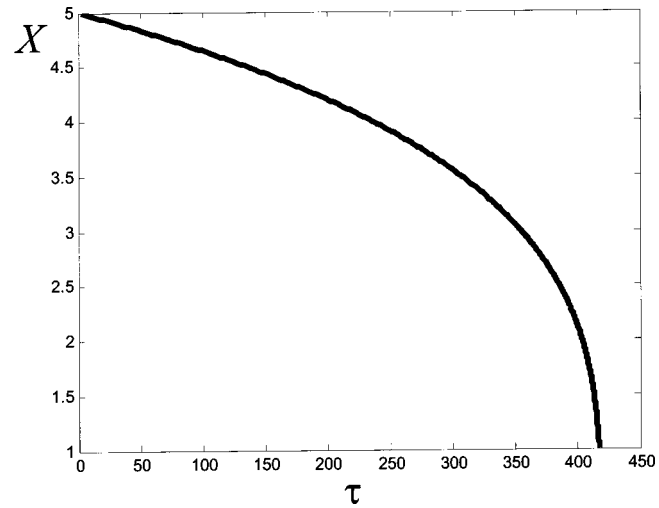

FIG. 11. The dimensionless position X of a sphere as a function of the dimensionless time when $X(0)=5$, $\varepsilon_2/\varepsilon_1=10$, and the potential of the plane $\phi=\Phi_0\sqrt{1-\cos\beta}$.

$$F_{x,\mathrm{DM}}\sim\frac{3\varepsilon_0\varepsilon_1(\varepsilon_1-\varepsilon_2)\pi\Phi_0^2}{8(2\varepsilon_1+\varepsilon_2)}\left[\frac{4r_2^3}{3d^3}+\frac{r_2^5}{3d^5}\right]+O(d^{-7}). \tag{71}$$

As in the planar case, the leading order terms $O((r_2/d)^3)$ in both the exact expression and the dipole-moment approximation are the same. The higher-order terms are, however, different.

We were not able to analytically obtain an approximation for the dielectrophoretic force when the particle is in close proximity to the wall. Instead, we solved the Fourier series. Since the convergence rate of the series deteriorates as the distance of the particle from the wall decreases, we exercised care to assure that a sufficient number of terms are retained in the series to assure appropriate precision of the results. Figure 10 depicts the normalized dielectrophoretic force as a function of $(X-1)^{1/2}$. The data points appear to neatly lie on a straight line indicating asymptotic behavior of the form $F_x\sim C_0+C_1(d-r_2)^{1/2}$, where $C_0\approx155.51$ and $C_1\approx-2.60\times10^3$. The constant C_0 can be estimated by extrapolating the straight line to $(X-1)=0$. In contrast to the planar case, the polarization force approaches a constant value as the distance between the particle and the surface decreases.

F. The dielectrophoresis of a spherical particle toward a plane wall

Finally, we examine the dielectrophoresis of a sphere in the vicinity of a plane wall. Happel and Brenner[21] provide an expression for the drag force acting on a sphere moving slowly perpendicular to a plane wall:

$$D_x=-6\pi\mu\dot{d}r_2\lambda, \tag{72}$$

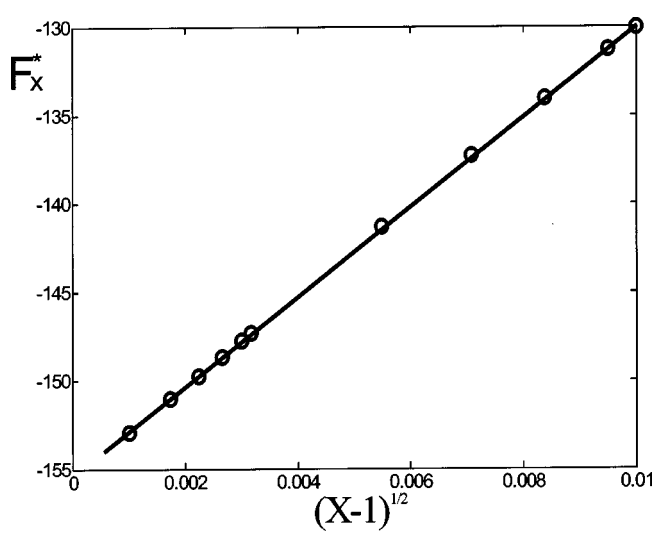

FIG. 10. The normalized DEP force on the sphere as a function of $(X-1)^{1/2}$ when $\varepsilon_2/\varepsilon_1=10$ and the surface potential is $\phi=\Phi_0\sqrt{1-\cos\beta}$. The circles correspond to the numerical calculations.

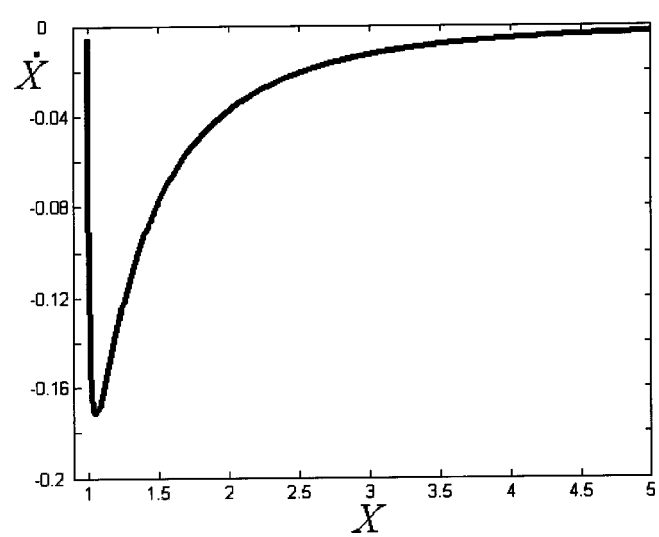

FIG. 12. The dimensionless velocity $\dot{X}$ of a sphere as a function of X when $X(0)=5$, $\varepsilon_2/\varepsilon_1=10$, and the potential of the plane $\phi=\Phi_0\sqrt{1-\cos\beta}$.

where

$$\lambda=\frac{4}{3}\sinh\varphi\sum_{n=1}^{\infty}\frac{n(n+1)}{(2n-1)(2n+3)}\times\left[\frac{2\sinh(2n+1)\varphi+(2n+1)\sinh 2\varphi}{4\sinh^2(n+1/2)\varphi-(2n+1)^2\sinh^2\varphi}-1\right] \quad (73)$$

and $\varphi=\cosh^{-1}(d/r_2)$. When the sphere is far from the wall, $\lambda\to 1$. Neglecting inertia and equating the viscous and electrostatic forces, we obtain the instantaneous velocity of the sphere in the x direction. The resulting ordinary differential equation is integrated numerically using a fourth-order Runge–Kutta algorithm.

Figure 11 depicts the dimensionless position $X(=d/r_2)$ of the sphere as a function of the dimensionless time (τ). The time scale is $8\mu r_2^2/(\Phi_0^2\varepsilon_0\varepsilon_1)$. The wall potential is $\phi=\Phi_0\sqrt{1-\cos\beta}$ and $\varepsilon_2/\varepsilon_1=10$. Figure 12 depicts the dimensionless instantaneous velocity as a function of the distance from the plane under the same conditions as in Fig. 11. Similar to the planar case, the velocity of the particle increases as it approaches the wall, attains a maximum, and then slows down to zero upon contact.

When the particle is far from the wall[21] ($d/r_2\to\infty$), the drag force is independent of d,

$$D_x\sim 6\pi\mu r_2\dot{d}\left(1+\frac{9r_2}{8d}\right), \quad (74)$$

and the velocity scales like d^{-3}.

In close proximity to the wall ($d-r_2\ll r_2$),[22]

$$D_x\sim\frac{6\pi\mu r_2^2\dot{d}}{(d-r_2)}, \quad (75)$$

and, as in the planar case, the velocity scales like $(d-r_2)$.

G. Conducting sphere next to an infinite wall

The case of the conducting sphere can be obtained as the limiting case of $\varepsilon_2/\varepsilon_1\to\infty$ in the derivation described in the previous subsection. Alternatively, one can proceed directly and develop somewhat simplified expressions. When the sphere is conducting, its potential is uniform. The electrical potential in the medium when the sphere conducts is

$$\phi_1=\sqrt{\cosh\alpha-\cos\beta}\sum_{n=0}^{\infty}\left[\frac{2\sqrt{2}\sin(n+\frac{1}{2})\alpha}{e^{(2n+1)\alpha_2}-1}V+F_n\frac{e^{(2n+1)\alpha_2}-e^{(2n+1)\alpha}}{e^{(2n+1)\alpha_2}-1}e^{-(n+1/2)\alpha}\right]P_n(\cos\beta). \quad (76)$$

The uniform electrical potential (V) of the sphere is determined from the condition of its electrical neutrality. When $\phi=\Phi_0\sqrt{1-\cos\beta}$,

$$V=\frac{2\Phi_0\cosh\frac{\alpha_2}{2}(\sqrt{\cosh\alpha_2+1}-\sqrt{\cosh\alpha_2-1})}{1+2\sqrt{2}\sinh\alpha_2\int_{-1}^{1}\frac{1}{\sqrt{\cosh\alpha_2-t}}\left(\Sigma_{n=0}^{\infty}\left(n+\frac{1}{2}\right)\frac{\cosh(n+\frac{1}{2})\alpha_2}{e^{(2n+1)\alpha_2}-1}P_n(t)\right)dt}. \quad (77)$$

The x-direction electrostatic force using the Maxwell stress tensor method is given by

$$F_x=\frac{2\sqrt{2}\pi\varepsilon_0\varepsilon_1V\Phi_0e^{\alpha_2}(e^{\alpha_2}+1)^2}{(e^{\alpha_2}-1)(e^{3\alpha_2}-1)}-\frac{2\pi\varepsilon_0\varepsilon_1\Phi_0^2e^{\alpha_2}}{(e^{\alpha_2}-1)^2}+4\pi\varepsilon_0\varepsilon_1V^2\sum_{n=0}^{\infty}\left[\frac{(e^{2\alpha_2}-1)e^{(2n+1)\alpha_2}[(1+n)(e^{2\alpha_2}-e^{(2n+1)\alpha_2})+n(e^{(2n+3)\alpha_2}-1)]}{(e^{(2n+1)\alpha_2}-1)^2(e^{(2n-1)\alpha_2}-1)(e^{(2n+3)\alpha_2}-1)}\right]. \quad (78)$$

The forces calculated with Eq. (78) are depicted with the plus symbol in Fig. 8, and they are nearly identical to the force values obtained when $\varepsilon_2/\varepsilon_1=100$ (not shown).

V. CONCLUSIONS

The dielectrophoretic forces acting on cylindrical and spherical particles embedded in perfectly dielectric viscous fluids confined in cylindrical/spherical shells and in semi-infinite media were calculated analytically as functions of the locations of the particles. The forces were exactly calculated using the Maxwell stress tensor and the concept of virtual work and approximately using the dipole-moment approximation. When the characteristic length of the electric field was larger than ten times the diameter of the cylindrical particles (twice the diameter of the spherical particles), the dipole-moment approximation estimated the dielectrophoretic force in the direction that is parallel to the line connecting the centers of the cylinders/spheres with better than 3% accuracy. As the characteristic length of the electric field increased, the accuracy of the dipole-moment approximation improved. Disturbingly, the dipole-moment approximation estimated nonzero forces in the other directions when no such forces existed.

The dielectrophoretic velocities of the particles were calculated under creeping flow conditions. As the particle approached the plane wall, its velocity increased, achieved a maximum, and then decayed to zero. The maximum velocity

occurred when the center of the particle was about distance $1.2r_2$ from the planar wall. In close proximity to the wall, the velocity was proportional to the gap thickness $(d-r_2)$ between the particle and the wall. The expressions derived here can also be used to estimate the migration time of the particles.

ACKNOWLEDGMENT

The authors acknowledge partial support from the DARPA SIMBIOSYS program N66001-01-C-8056.

[1]H. A. Pohl, *Dielectrophoresis: The Behavior of Neutral Matter in Nonuniform Electric Fields* (Cambridge University Press, New York, 1978).
[2]T. B. Jones, *Electromechanics of Particles* (Cambridge University Press, Cambridge, 1995).
[3]P. A. Smith, C. D. Nordquist, T. N. Jackson, T. S. Mayer, B. R. Martin, J. Mbindyo, and T. E. Mallouk, ''Electric-field assisted assembly and alignment of metallic nanowires,'' Appl. Phys. Lett. **77**, 1399 (2000).
[4]N. G. Green and H. Morgan, ''Dielectrophoresis of submicrometer latex spheres. I. Experimental results,'' J. Phys. Chem. B **103**, 41 (1999).
[5]N. Markarian, M. Yeksel, B. Khusid, K. Farmer, and A. Acrivos, ''Limitations on the scale of an electrode array trapping particles in microfluidics by positive dielectrophoresis,'' Appl. Phys. Lett. **82**, 4839 (2003).
[6]S. B. Asokan, L. Jawert, R. L. Carroll, R. E. Chene, S. Washbur, and R. Superfine, ''Two-dimensional manipulation and orientation of actin-myosin systems with dielectrophoresis,'' Nano Lett. **3**, 431 (2003).
[7]M. Washizu and O. Kurosawa, ''Electrostatic manipulation of DNA in microfabricated structures,'' IEEE Trans. Ind. Electron. **26**, 1165 (1990).
[8]R. Krupke, F. Hennrich, H. V. Lohneysen, and M. M. Kappes, ''Separation of metallic from semiconducting-single-walled carbon nanotubes,'' Science **301**, 344 (2003).
[9]T. B. Jones, ''Dielectrophoretic force calculation,'' J. Electrost. **6**, 69 (1979).
[10]T. B. Jones and M. Washizu, ''Multipolar dielectrophoretic and electrorotation theory,'' J. Electrost. **37**, 121 (1996).
[11]L. Benguigui and I. J. Lin, ''More about the dielectrophorectic force,'' J. Appl. Phys. **53**, 1141 (1982).
[12]J. A. Stratton, *Electromagnetic Theory* (McGraw, New York, 1941).
[13]P. Moon and D. E. Spencer, *Field Theory Handbook* (Springer, Berlin, 1971).
[14]J. D. Jackson, *Classical Electrodynamics* (Wiley, New York, 1998).
[15]M. Zahn, *Electromagnetic Field Theory: A Problem Solving Approach* (Wiley, New York, 1979), pp. 273–277.
[16]D. J. Jeffery and Y. Onishi, ''The slow motion of a cylinder next to a plane wall,'' Q. J. Mech. Appl. Math. **34**, 129 (1981).
[17]A. Goyette and A. Navon, ''Two dielectric spheres in an electric field,'' Phys. Rev. B **13**, 4320 (1976).
[18]H. H. Bau, ''Temperature distribution in and around a buried heat generating sphere,'' Int. J. Heat Mass Transfer **25**, 1701 (1982).
[19]FEMLAB is a product of COMSOL AB, Sweden.
[20]R. Tao, Q. Jiang, and H. K. Sim, ''Finite-element analysis of electrostatic interactions in electrorheological fluids,'' Phys. Rev. E **52**, 2727 (1995).
[21]J. Happel and H. Brenner, *Low Reynolds Number Hydrodynamics* (Martinus Nijhoff, The Hague, 1983).
[22]D. Y. C. Chan and R. G. Horn, ''Drainage of thin liquid films,'' J. Chem. Phys. **83**, 5311 (1985).

Physics of Fluids is copyrighted by the American Institute of Physics (AIP).
Redistribution of journal material is subject to the AIP online journal license and/or AIP copyright. For more information, see http://ojps.aip.org/phf/phfcr.jsp
Copyright of Physics of Fluids is the property of American Institute of Physics and its content may not be copied or emailed to multiple sites or posted to a listserv without the copyright holder's express written permission. However, users may print, download, or email articles for individual use.